What makes a dangling bond a binding site for thermal CH_3 radicals? – A combined molecular dynamics and potential energy analysis study on amorphous hydrocarbon films

P.N. Maya [a], U. von Toussaint and W. Jacob

Max-Planck-Institut für Plasmaphysik, EURATOM Association, Boltzmannstr. 2, D-85748 Garching, Germany

Identification of dangling bonds on amorphous films is not as straight forward as in the case of crystalline materials. The task is further complicated in the case of amorphous hydrocarbon (a-C:H) films by the existence of a wide variety of atomic arrangements. We present a technique based on potential energy analysis of a-C:H films to identify dangling bonds and physisorption sites. However, molecular dynamics simulations of the sticking of thermal CH_3 on a-C:H surfaces show that not all dangling bonds are binding sites for a CH_3 radical. Furthermore, the total sticking coefficient of the surface is not solely linked to the number of dangling bonds and can even decrease for the same number of dangling bonds because the carbon atoms that possess a binding site, *active carbon atoms*, show drastically different reactivity towards CH_3. The reactivity of active carbon atoms is decided by (a) their type, which is decided by the bonding partners, (b) their distance from the local surface and (c) the local environment. The reactivity of the active carbon atoms can be largely increased by energetic ion bombardment due to hydrogen depletion and local rearrangement.

PACS numbers: 68.43.Fg, 82.20.Wt, 68.55.at, 82.65.+r

[a] Corresponding author email: pnmaya@ipp.mpg.de

Present address: Max-Planck-Institut für Astrophysik, Karl-Schwarzschild-Str.1, D-85748 Garching, Germany

I. INTRODUCTION

Amorphous hydrogenated carbon (a-C:H) films – often also termed diamond-like carbon films – are a fascinating class of amorphous materials with an amazing variety of forms and physical properties [1, 2]. The great interest in these types of films was and is triggered by their extraordinary material properties which are of great interest for a wide range of technological applications such as protective coatings in magnetic storage technology [3–5], tribological coatings in the automotive industry [5], optical coatings [6], and quite importantly as bio-compatible coatings for various medical applications [5, 7]. These films are routinely manufactured using plasma-enhanced chemical vapor deposition from hydrocarbon precursor gases [2, 8, 9]. Similar conditions prevail in the cold edge of magnetically confined nuclear fusion plasmas where also the growth of hydrocarbon films was observed due to the erosion of carbon first-wall materials [10, 11].

In such low-temperature plasmas the precursor gas is ionized and dissociated, and carbon-carrying radicals and ions as well as hydrogen atoms and ions impinge on the surface [8, 12]. The observed film growth is the net result of various deposition and erosion processes triggered by the different particle species. These processes are not entirely independent and clear evidence for the existence of synergisms have been found [13]. For example, in particle-beam experiments using independently controllable radical sources for atomic hydrogen atoms and CH_3 radicals it was shown that the simultaneous interaction of both species leads to a much higher sticking probability for the methyl radical than irradiation with CH_3 alone [12, 14, 15]. Similarly, ion bombardment was also found to increase the sticking probability of CH_3. These results were explained by the abstraction or displacement, respectively, of surface atoms, thereby creating an active surface site, often termed a *dangling bond*. The CH_3 radicals are assumed to directly stick on these dangling bonds. In this picture the steady-state dangling bond coverage of the surface determines the sticking probability of CH_3 and thus the growth rate. Rate equation models that account for the dangling bond creating and consuming processes could very well reproduce the growth rates in the parameter range investigated in these experiments [13, 16–18].

Modeling the evolution of the structure during the a-C:H film growth is inherently a multi-scale problem. Monte Carlo (MC) methods with parametrized sets of reaction probabilities for various processes involving both CH_3 radicals and ions have been used in the past to model the film structure [19–22]. The reaction probabilities are derived based on the input from both experiments and lower scale models such as molecular dynamics and *ab initio* calculations. *Ab initio* calculations are able to model the formation and the electronic structure and properties of dangling bonds on well-defined surfaces of a few atoms [23, 24]. For amorphous film growth this will not be representative due to the large number of atomic arrangements. Molecular dynamics (MD) simulations can bridge this gap by still resolving dynamic details of the atomistic processes while being able to treat considerably larger systems and hence provide the required input for the structural MC growth models.

MD simulations have been used extensively in the past for studying the sticking of hydrocarbon radicals on a-C:H surfaces [25–35]. The influence of the orientation of the radical was studied by Sharma et al. [36]. The effect of hydrogen flux in the sticking probabilities of hydrocarbon radicals on a-C:H surface was investigated by *deRooij et al.*, using Brenner potential at 700 K and 1000 K sample temperatures [29]. The sputtering and deposition of hydrocarbon films by C_2H_2 radicals were studied by *Jäger et al.* at high impinging energies of the radical [35]. The intrinsic stress generated due to ion bombardment was also investigated in such films [33, 34]. The growth of diamond-like carbon films from different low energy (<2 eV) radical species, mainly C_2H_2, was investigated by *Neyts et al.* using Brenner potential [30].

The sticking cross-section for the chemisorption of methyl radicals on specific dangling bond locations on the diamond surface were studied by *Träskelin et al.*, using both classical MD and a tight binding approach [37–39]. In these simulations a dangling bond was created by removing a hydrogen atom from a fully hydrogen-terminated surface. It was shown that the cross-section depends on the local environment of the dangling bonds. The simulations also showed that for low energy radicals (corresponding to a thermal distribution of 2100 K distribution) no sticking was observed on the fully hydrogen terminated surface.

MD simulations of the sticking probability of CH_3 radicals on reconstructed diamond surfaces were performed by *Alfonso et al.*[40, 41] for energies above 1 eV at different incident angles. It was observed that the sticking probability increases with the incident energy and reduces with both the angle of incidence with respect to the surface normal and the surface hydrogen content. The decrease of sticking probability with surface hydrogen content was explained by the reduction of the available reactive sites on the surface and the steric hindrance due to the surface hydrogen, which enhances the reflection of the incoming radicals. These studies significantly improved our understanding of the growth of a-C:H films from CH_3 radicals. However, realistic a-C:H films differ from the studied model cases – well defined isolated dangling bonds on a diamond surface – in several respects. They have inherently rough surfaces and dangling bonds are present in a wide variety of atomic neighborhoods.

In this article we study the role of dangling bonds in the sticking of CH_3 radicals on realistic a-C:H surfaces using classical MD simulations. Surfaces with different sticking probabilities are created using the same instruments as in the particle beam experiments, namely atomic hydrogen exposure and ion bombardment. Identifying dangling bonds on these surfaces is by far not as straight forward as on well-defined diamond surfaces. We tackle this problem by potential energy analysis of the films using a hydrogen atom as a test particle and applying appropriate selection rules for dangling bond identification. Not all the identified dangling bonds show sticking, and the reactivity of those that do, has a large variation. By detailed characterization of the local environment we investigate what determines the reactivity of a dangling bond.

The article is organized as follows: the MD simulations and their results are discussed in Sects. II and III. The scheme to

identify the active carbon atoms is presented in Sect. IV and the discussion is in Sect. V.

II. MD SIMULATIONS

The simulations were carried out using the molecular dynamics code, HCParcas (Hydrocarbon Parallel Cascade) [42]. It uses a fifth-order predictor-corrected Gear algorithm to calculate the positions and velocities of particles using adaptive time-steps. The Brenner potential was used to model C-C and C-H interactions [43–45]. The potential has been compared with tight binding, *ab initio* and DFT based calculations in the past by various authors [39, 46–48]. These studies show that the Brenner potential is capable of describing short-range interactions accurately. It was shown by Sharma et al., that the Brenner potential can qualitatively describe the sticking of hydrocarbon radicals on a-C:H surfaces [36]. Träskelin et al. have compared the sticking of CH_3 radicals between the Brenner potential and a tight-binding approach based on a second order expansion of the KohnSham total energy in density functional theory with respect to charge density fluctuations [39]. This study also shows that the sticking cross-sections have a qualitative match in both the cases. Hence, the computationally efficient classical Brenner potential appears adequate for the description of the present system.

The simulation has three parts: creation of an a-C:H film, preparation of different surfaces and bombardment with CH_3 radicals.

A. Sample Generation

The a-C:H sample was created by repeated annealing and cooling of a random collection of carbon and hydrogen atoms. The details of sample preparation are described in [49]. Periodic boundary conditions were used along the *X* and *Y* directions and a free boundary was used along the *Z* direction.

The sample consists of 916 atoms (572 carbon atoms and 344 hydrogen atoms) and has a size of $1.4 \times 1.5 \times 2.7$ nm^3. The density is ~ 1.7 g cm^{-3} and the hydrogen content ($H/(H+C)$), is 0.375. For hydrocarbon films formed from ethane plasma discharges similar values of H content (0.39) and density (1.7 g cm^{-3}) have been reported [9]. The amorphous nature of the film was characterized by the radial distribution function (RDF) of the carbon atoms [49] and is in good agreement with the data obtained from neutron scattering experiments [50]. The numbers of three-fold and four-fold coordinated carbon atoms are 60 % and 37 %, respectively. This is in agreement with the properties of films which are intermediate between hard and soft [2]. Atoms within a distance of 0.3 nm of the bottom of the cell were fixed to mimic the effect of an underneath bulk layer. The fixed layer consisted of 64 carbon atoms and 36 hydrogen atoms. From now onwards these atoms are not included in computing any

of the sample properties. Thus the number of carbon and hydrogen atoms that are used for computing the sample properties is 508 and 308, respectively. We call this the *virgin sample*.

B. Surface Preparation

Three types of sample surfaces were created by bombarding the virgin sample by either hydrogen or argon atoms. Bombarding the virgin sample by one hundred hydrogen atoms of 0.5 eV energy results in an increase in the total number of hydrogen atoms of the sample from 308 to 316. Almost all of these hydrogen atoms were incorporated within a distance of 0.8 nm from the topmost atom location of the virgin sample. We call this *H-exposed sample*.

By continuing the hydrogen bombardment up to 500 H atoms, we created an *H-saturated sample*. The total number of H atoms increased to 329 and the added hydrogen distribution is limited to the top 0.8 nm which is similar to the H-exposed sample.

The *Ar-bombarded sample* was created by bombarding 14 Ar atoms of 100 eV energy on the virgin sample. The argon bombardment resulted in the sputtering of bound H atoms from the film within a distance of 1.2 nm from the topmost atom location of the virgin sample.

The properties of the samples are summarized in Tab. I. The range of 100 eV Ar atoms within the sample is 1.2 nm and the damage creation and hydrogen elimination happened within this range [49]. Hence, the H content of this 1.2 nm thick surface region is calculated and is referred to as H_{top}.

TABLE I. Properties of the samples. $(\mathrm{H}/(\mathrm{H}+\mathrm{C})$ is the hydrogen content of the complete sample (neglecting the atoms in the fixed layer at the bottom of the sample). The H content of the top 1.2 nm of the film is referred to as H_{top}.

Number	Sample	C	H	$\mathrm{H}/(\mathrm{H}+\mathrm{C})$	H_{top}
1	Virgin	508	308	0.377	0.39
2	H-exposed	508	316	0.383	0.41
3	H-saturated	508	329	0.393	0.45
4	Ar-bombarded	507	299	0.370	0.37

C. CH_3 Bombardment Simulations

The a-C:H samples were bombarded by CH_3 radicals at normal incidence. The incident energy of the radicals is chosen in a such a way that the impinging radical can neither modify the sample structure nor create new dangling bonds on the surface due to kinematic effects. This is an important criterion since we want to understand the sticking on already existing features of the surface. Thus the incident energy was sampled from a Boltzmann velocity distribution corresponding to 2000 K. This corresponds to a mean energy of $\sim$ 0.25 eV which is much less than C–C or C–H bond energy ($\sim$ 2 eV). The CH_3 radicals were created by specifying the coordinates of C and H atoms in sp^2 (planar) configuration and then relaxed afterwords for about 0.5 ps. The velocity of the molecule was specified by the velocity of the center of mass of the molecule and the velocities of the atoms in the center of mass frame (rotational and vibrational temperature). Ten thousand non-cumulative bombardment events homogeneously distributed on a flat area of 1.10 nm^2 were performed in all the simulations. This gives reasonably good statistics for the estimation of reaction events at the surface sites. The sample temperature was brought down to 300 K after every bombardment. This was achieved by using the Berendsen thermostat [51] where temperature control was applied to the border regions of 0.2 nm along each direction. The actual area of bombardment excludes this thermostated region. The velocities of the atoms in the thermostated area are scaled by a factor

$$\lambda = \sqrt{1 + \frac{\Delta T}{\tau}\left(\frac{T_0}{T} - 1\right)} \tag{1}$$

where T_0 is the desired temperature and T is the temperature of the atoms which lay outside the thermostated region. The rise time of the thermostat is given by τ which decides how fast the system can reach the desired temperature. Every impact of a CH_3 was followed by 10 ps relaxation. Each bombardment event corresponds to about 80 minutes of computational time resulting in about 40 days of computation on an IBM blade system of 56 processors (Intel Xeon(R)), each having a RAM of 2 GB and a clock speed of 3.0 GHz.

III. RESULTS

We found mainly three types of reactions in the bombardment simulations: (a) reflection of the incident CH_3, (b) abstraction of bound hydrogen from the surface and (c) direct sticking of the radical on the surface. Table II lists the occurrences of these events. They are classified based on the position and the potential energy of the carbon atoms of the CH_3 at the end of the simulation. The potential energy of the C atom in an isolated CH_3 molecule in the Brenner potential is approximately -6 eV and for a fully co-ordinated carbon atom it is $\sim$ -8 eV. Hence, the carbon atoms of all the incident CH_3 that have a potential energy of approximately -8 eV and are located within a distance of 0.3 nm from the topmost atom location are considered as

TABLE II. Surface reactions of the four different samples for the impact of thermal CH_3 radicals with $T = 2000$ K. The hydrogen content of the top 1.2 nm of the films is (H_{top}).

Sample	H_{top}	Events (out of 10,000)			Average Sticking coefficient (η_{MD})
		Reflection	H abs.	Sticking	
Virgin	0.39	9864	14	122	$(1.2\pm1.1)\times10^{-2}$
H-exposed	0.41	9899	17	84	$(8.4\pm0.9)\times10^{-3}$
H-saturated	0.45	9980	7	13	$(1.3\pm0.4)\times10^{-3}$
Ar-bombarded	0.37	9474	1	525	$(5.3\pm0.2)\times10^{-2}$

sticking. If the carbon atoms of the CH_3 have a potential energy of ~ -8 eV and are located 0.3 nm above the topmost atom of the sample then a CH_4 molecule is formed and the corresponding events are H-abstraction events. The CH_4 molecule formation was additionally confirmed by checking that the distance between the four H atoms and the central carbon atom of the molecule is within 0.12 nm (the C–H bond length for Brenner potential is ~ 0.11 nm). The rest of radicals is considered as reflected. From Tab. II, we see that most of the radicals are reflected from the surface and a very few of the radicals abstracted a surface bound hydrogen atom.

We have not observed any evidence of surface diffusion of the incoming radicals within the time scale of our simulations. The mechanism of the growth of a-C:H films from thermal CH_3 radicals is the direct sticking of the radicals on the surface. We have also not observed any break-up of the CH_3 during the incorporation.

A series of snapshots of one CH_3 sticking event on the virgin surface is shown in Fig. 1. The incoming radical is encircled. At 380 fs (Fig. 1a) a planar CH_3 radical approaches the surface. In Fig. 1b at 510 fs we can see that the radical has changed its orientation. At 540 fs (Fig. 1c) it gets attached to the surface of the film and in Fig. 1d the radical has rotated around the C–C bond axis. This rotation continues until the local relaxation is completed.

The C atom locations of the stuck CH_3 radicals ('CH_3 locations') within the film for the virgin sample (a) and the Ar-bombarded sample (b) are shown in Fig. 2. Each indicated CH_3 location corresponds to a single sticking event observed in one of the 10,000 non-cumulative bombardment simulations. The CH_3 locations are not evenly distributed across the sample surface. However, it appears that some locations are more favorable for sticking than others.

From Tab. II, we see that the number of sticking events decreases with the increase in H_{top}, the hydrogen content in the top 1.2 nm of the film. The average sticking coefficient (η_{MD}) is defined as the ratio of the number of sticking events to the total

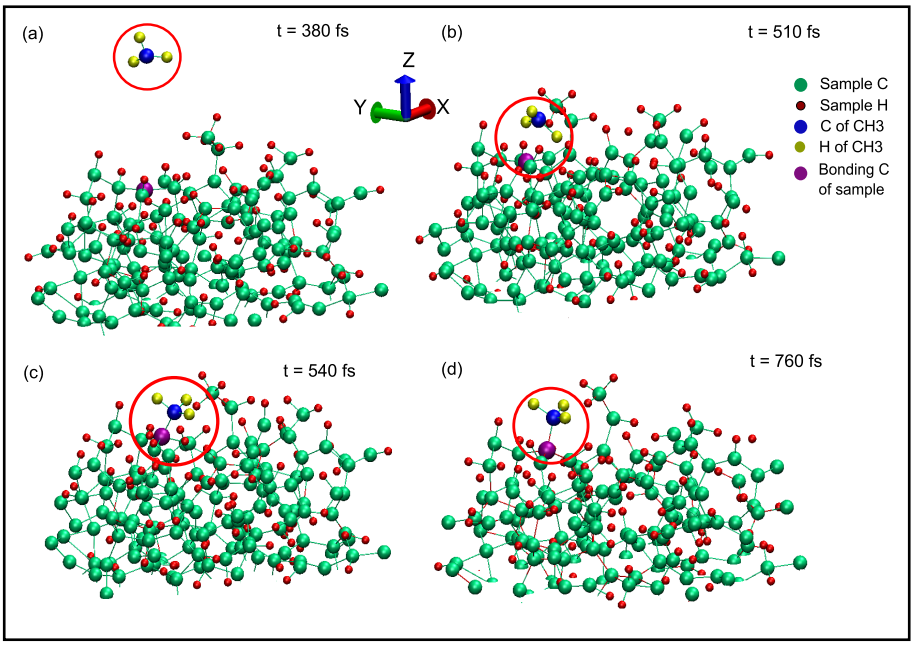

FIG. 1. Snapshots of a single CH_3 (circled) sticking event on the virgin sample at 300 K. (color online)

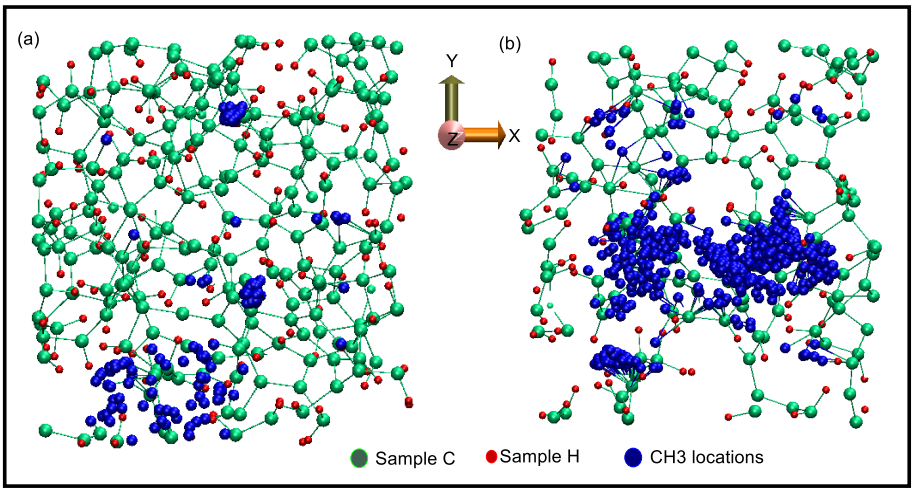

FIG. 2. Birds-eye view of the C atom locations of the stuck CH_3 radicals (CH_3 locations) in the film. (a): virgin sample, (b): Ar-bombarded sample. For details see text. (color online)

number of incident radicals. For the virgin sample it is 1.2×10^{-2}, which drops down to 1.3×10^{-3} for the H-saturated sample. In the case of the Ar-bombarded surface, the sticking coefficient was found to be 5.3×10^{-2}, which is the highest among the four samples that we have used.

The sticking coefficients on the virgin and the Ar-bombarded surfaces are close to those reported for CH_3-H and CH_3-Ar^+ co-bombardment experiments [12, 14, 15, 17, 18, 52]. However, we would like to emphasize that none of the MD generated surfaces corresponds to any of the steady-state conditions in the particle beam experiments. As the virgin sample was not created

in a bombardment simulation, it is unclear what experimental steady-state it corresponds to. The H-exposed and the H-saturated samples show higher densities compared with the extremely soft surface synergistically grown in CH_3-H experiments. The Ar-bombarded sample corresponds to the state of the surface after Ar-only bombardment rather than the steady-state during combined CH_3-Ar^+ experiments. This could be the reason for the higher sticking coefficient observed in the case of the Ar-bombarded sample in our simulations compared with the experimental values.

The average sticking coefficient (η_{MD}) as a function of H_{top} is shown in Fig. 3. The sticking coefficient increases with the decreasing H_{top}. This is in agreement with the previous observations on diamond surfaces [39, 40]. A tentative explanation for the observed correlation can be given in terms of the number of dangling bonds within the film. There exists a certain number of dangling bonds in the case of the virgin sample. Once hydrogenated they are no longer available for sticking which is the case for both the hydrogenated samples. The Ar-bombardment creates additional dangling bonds available for sticking by C–C bond breaking and sputtering of H and C atoms.

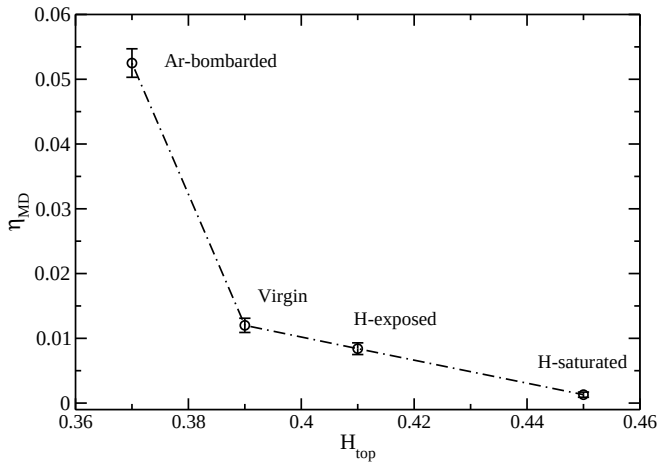

FIG. 3. The sticking coefficient (η_{MD}) as a function of the hydrogen content of the top 1.2 nm layers of the sample (H_{top}).

Although MD simulations contain all the information about the system at any instant in time, due to the inherent complexity of the hydrocarbon network it becomes difficult to identify the dangling bonds using conventional MD simulations. Therefore, we use potential energy analysis to identify the dangling bonds and the possible binding sites for CH_3. We will refer to a carbon atom of the sample that can be associated with a binding site for CH_3 as 'active carbon atom'.

IV. IDENTIFICATION OF 'ACTIVE CARBON ATOMS'

A method is devised for identifying the active carbon atoms based on the idea that they are attractive potential locations within the film. The proposed method has three parts: (1) calculation of the potential energy of a test hydrogen atom within the sample at regular grid points, (2) elimination of certain sites according to the potential energy values of the neighboring grid points and (3) assignment of the site to a sample carbon atom. The details of the method are discussed in the following sections.

A. Potential Energy Analysis (PEA)

The potential energy (PE) was calculated by dividing the sample into a three dimensional grid and calculating the PE of the H atom at the grid points. The grid-size was varied between 0.01 nm to 0.1 nm and it was found that up to 0.05 nm, the potential energy variation is relatively smooth. Hence, in our calculations we have kept the grid size of 0.05 nm. The reason for choosing H atoms as test particles is two fold: first, as CH_3 radicals, H atoms can only make σ bonds with C atoms. This is, *e.g.*, not the case for C atoms as they can also make π bonds with other C atoms (such as sp^2 type and sp type). Second, unlike for CH_3 radicals, there is no orientation preference [36] for H atoms and this makes calculations relatively simple and fast. The sample atoms were at fixed locations ('frozen' in time, no local relaxation of the sample) while calculating the potential energy.

B. Definition of the Surface of the Films

Due to the inherent roughness on the atomic scale, there exists no unique definition of the surface of amorphous films. We model the surface as the transition region above the film where the gas-phase particles start to feel the attractive potential of the atoms constituting the film. In the Brenner potential the cut-off distance for C-H and H-H interactions is 0.18 nm and 0.17 nm respectively. Hence this surface is composed of spheres of 0.18 nm radius around each C atom and 0.17 nm radius around each H atom. To find the surface we have used the potential energy analysis as a tool. The potential energy of the test H atom is scanned downwards starting from above the sample. The finer grid size of 0.01 nm is used to generate smooth surfaces for a better visual appearance. As surface we define for every X–Y coordinate the lowest Z coordinate where the potential energy of the H atom is lower than 10^{-5} eV.

The surface thus obtained is rough and the roughness is defined as the mean square deviation of the height from the mean value. The surface area is calculated using triangulation. The flat area (assuming no roughness) of the surface is 2.10 nm^2. All the four surfaces have an area much larger than the flat area. While the hydrogenated surfaces are rather similar to the virgin sample, the Ar bombardment tends to roughen the surface further and both the roughness (0.191 nm) and the surface area

(5.38 nm^2) are increased by a factor of 1.3 compared to the virgin surface (roughness = 0.152 nm and area = 4.15 nm^2).

C. Algorithm for Identifying Active Carbon Atoms

Not every attractive PE location for hydrogen constitutes a binding site for a CH_3 radical or a dangling bond of its own. The extent of the attractive region for C–H interaction is 0.18 nm in the Brenner potential [43]. Hence this number should also determine the typical size of a dangling bond's attractive region. With our spacing of 0.05 nm, many grid points lie in this region. Since every dangling bond belongs to exactly one carbon atom, we can alternatively try to find the carbon atoms associated with the dangling bonds. For this purpose we have devised the following algorithm:

- Step 1: Determine the potential energy of the test H atom within the sample on a 0.05 nm spaced grid.
- Step 2: Find all the attractive grid points (PE < 0).
- Step 3: Among the attractive grid points identify those that are surrounded solely by attractive grid points, i.e. that are in the center of a cube of 26 neighboring grid points ($3^3 - 1$) for all of which PE < 0.

In step 3, the neighborhood criterion helps to eliminate many attractive grid points that belong to the same dangling bond and leaves only a few central ones. All those central sites are associated with the neighbouring carbon atom. This means, more than one central point may be associated with a given carbon atom. In this calculation, due to the discrete grid we may not probe the exact potential minimum corresponding to a dangling bond. Nevertheless, the lowest potential energy value among the grid points associated with one carbon atom can be taken as an estimate of the strength of its attraction. We see that this value varies between -0.3 eV to -1.7 eV. We find that 130 carbon atoms with such sites are present throughout the virgin sample. However, from the MD data, we see that sticking happens only close to the surface of the sample. Hence we introduced an additional criterion to eliminate those grid points that are buried in the sample in step 4. The algorithm now is:

- Step 4: Among the attractive central grid points (x, y, z) reject those that have PE > 0 at any of the grid points above $(x, y, z' > z)$.
- Step 5: Associate the identified grid points of step 4 to the nearest carbon atom within the sample.

This procedure yielded 40 candidates for active carbon atoms in the case of the virgin sample. However, from the analysis of the MD data, we see that sticking happens only on a few of them. In order to understand this discrepancy, we take into account the potential energy of the strongest attractive grid point associated with each carbon atom. These grid points have

either PE ≥ -0.6 eV or PE ≤ -0.9 eV. We find that sticking did not happen on those carbon atoms that have PE ≥ -0.6 eV. Since this corresponds to typical physisorption energies, we call them physisorption sites. The corresponding 21 carbon atoms that possess only physisorption sites are not considered any further.

This adds to the following step in the algorithm:

- Step 6: Reject those candidate carbon atoms that possess only a physisorption site (PE ≥ -0.6 eV).

The remaining 19 carbon atoms that possess grid points of energy less than -0.9 eV are called *candidate carbon atoms with dangling bonds*. Still, on a few of them no sticking was observed. Additionally, on those that showed sticking the number of sticking events was drastically different. In order to understand why, we have analyzed their individual neighborhood. We describe the neighborhood by the following notation: iCjH means the respective carbon atom has bonds to $i \in \{1,\ldots,3\}$ carbon and $j \in \{0,\ldots,3-i\}$ hydrogen atoms. We find active carbon atoms of all types except 1C. The remaining five types 1C1H, 1C2H, 2C, 2C1H and 3C are present in our films. For this classification, a carbon atom is considered to be bound to another carbon atom if the C–C distance is less than 0.16 nm and to a H atom if the C–H distance is less than 0.12 nm.

A vast majority of the first three types showed sticking on all the four samples. In contrast, there was sticking only on very few of the 2C1H and 3C types. A closer analysis revealed that all of the 3C and 2C1H types on which sticking happened were either part of a chain (flexible environment) or had a bond to another candidate carbon atom.

Hence, the following final step was added to the algorithm

- Step 7: Among all the candidate carbon atoms of 3C and 2C1H type reject those that are neither part of a chain nor have a bond to another candidate carbon atom.

The remaining candidate carbon atoms are called 'active' carbon atoms in the rest of the article. Eleven active carbon atoms are identified in the case of the virgin sample.

V. DISCUSSION

A. Virgin Sample

With the algorithm described in Sect. IV C eleven active carbon atoms are identified in the case of the virgin sample and sticking happened on nine of them. We assign a sticking event to a carbon atom if in the MD simulations the potential energy of the carbon atom of the sticking radical as well as of the binding sample carbon atom has decreased by more than 1 eV at the end of the simulations. Based on this criterion 121 out of 122 observed sticking events on the virgin sample are assigned to one of the

active carbon atoms. For all the 121 events the final C–C distance between the active carbon atom and the corresponding CH_3 location is less than 0.16 nm. The corresponding mean C–C distance is 0.155 ± 0.003 nm. For the one remaining sticking event we found that the decrease in potential energy of the radical's carbon atom is still more than 1.0 eV but for none of the surface carbon atoms did the potential energy change by more than 0.1 eV. For this event, the C–C distance between the CH_3 location and closest sample C atom is 0.2 nm. We call such sticking events 'weak' sticking. Such a sticking event is not associated with any carbon atom in our scheme.

Figure 4a shows an X–Y view of the positions of the active carbon atoms at beginning (numbered open circles) and end (solid circles) of the CH_3 bombardment simulations along with the CH_3 locations (small symbols) for the virgin sample. Figure 4b shows an X–Z view of the same data (for better visibility the final positions of active carbon atoms are not shown here). The association of sticking events with the respective active carbon atoms is shown in the legend. The labelling of the active C atoms is in the order of decreasing number of sticking events at each atom, i.e., the atom with the highest number of sticking events is labelled as number 1 and so on. The carbon atoms with no sticking (#10 and #11) are labelled in the order of increasing distance from the local surface. The only one weak sticking event in this sample is shown by the '+' symbol below the active atom #1. Although it appears to be close to the initial position of the active carbon atom #1, for this sticking event the atom #1 was at a distance of 0.2 nm from the CH_3 location at the end of the simulation.

Fig. 4b shows that almost all the CH_3 locations are above the corresponding active C atoms. Although the sample surface is bombarded homogeneously, the sticking on the surface and on individual active carbon atoms is very inhomogeneous. From both the Figs. 4a and 4b we find that while the sticking events corresponding to active carbon atoms #2 to #9 are rather localized, those associated with the active carbon atom #1 are distributed. The different behavior can be rationalized as follows: Due to thermal motion and relaxation of the hydrocarbon network, the final positions of the active C atoms can be different from their positions in the initial sample used for the PES analysis. This along with the thermal motion of the sticking CH_3 results in the scatter of the sticking positions. This is supported by the final positions of active carbon atoms after the sticking in Fig. 4a. The final positions of the active carbon atoms #2 to #9 are very close to their initial positions. The maximum movement of any of those carbon atoms for any sticking event was about 0.06 nm and the mean movement was about 0.04 nm.

Atom #1 is part of a flexible hydrocarbon chain consisting of 6 carbon atoms. This adds additional mobility to this atom and consequently its maximum (0.3 nm) and mean (0.19 nm) movement from the initial position was about 5 times higher compared to other active C atoms. This additional mobility results in a large number of sticking (36 out of 62) events where the active carbon atom #1 and the stuck CH_3 radical are located in the in the non-bombarded thermostated region at the end of the simulations (Fig. 4a). An enlarged view of the active carbon atom #1 and all the associated CH_3 locations is shown in Fig. 4c. A

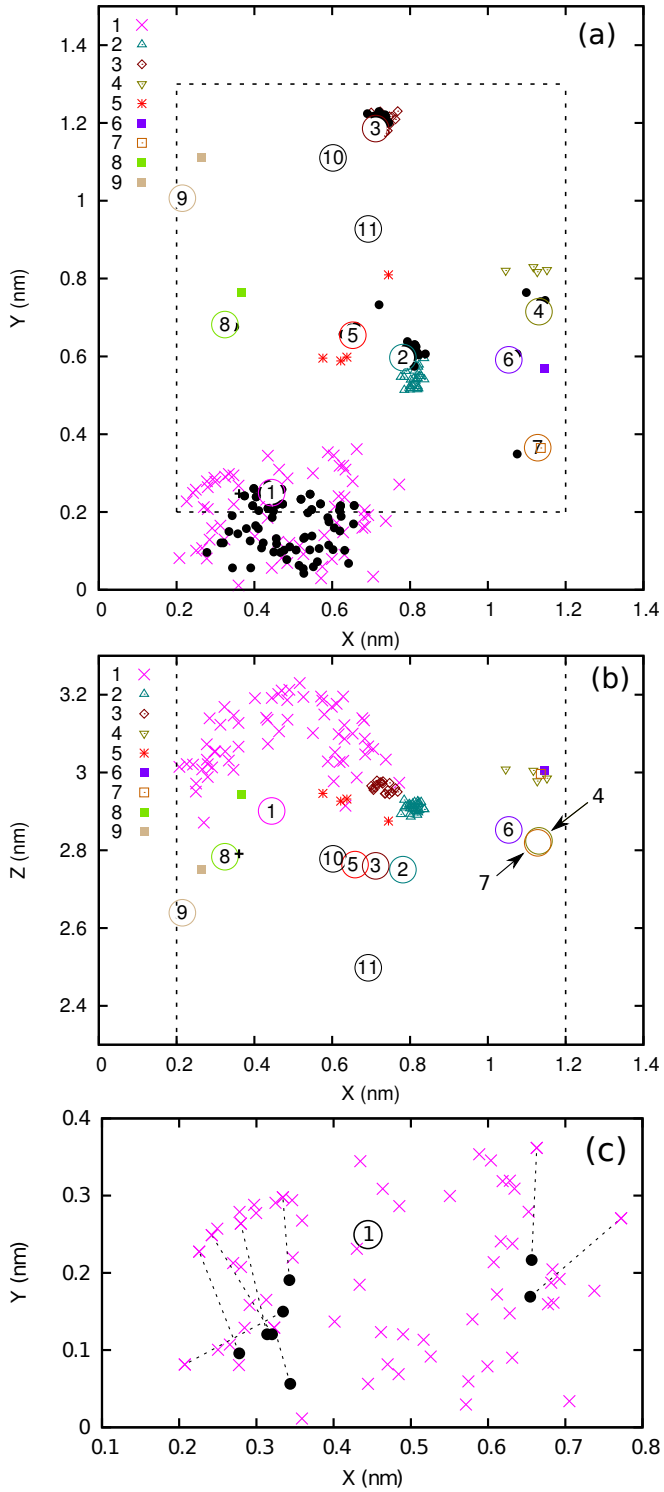

FIG. 4. (a) X–Y representation (birds-eye view) of the identified active carbon atoms (open circles with numbers), CH_3 locations (small symbols) and final position of active carbon atoms (solid circles) at the end of the simulations for the virgin sample. The region outside the dashed rectangle is the thermostated area that was not bombarded by CH_3. The association of sticking events to the active carbon atoms is shown in the legend. The weak sticking event is shown as '+' symbol. (b) X–Z view of the above data with out the final positions of active carbon atoms. (c) An enlarged view of the active carbon atom #1 along with all CH_3 locations. The solid circles represent selected extreme positions of the active atom #1 at the end of the simulations. Their attribution to the corresponding sticking events is shown by dotted lines.

few selected final positions of this carbon atom and their association with the corresponding sticking events are shown by dotted lines. Although the carbon atom moves considerably from its initial position, the largest final distance between the atom #1 and the radical's C atom is 0.158 nm which is well within the range of C–C bond lengths (0.155±0.003) observed in the sample.

A 3D view of the complete static surface of the virgin sample along with the CH_3 locations (small solid dots) is plotted in Fig. 5. At the end of the simulations a majority of the sticking locations (77 out of 122) were above the initial surface (solid circles in Fig. 5). The sticking in the "valleys" of the surface is localized, i.e., for active C atoms #2 to #5. In contrast, the CH_3 locations belonging to the active carbon atom #1 that forms a local "hill" of the surface are much more distributed. This is the consequence of two effects. First, as the bond length is constant there are more possible orientations of the stuck CH_3 with respect to the active carbon atom on a hill than in a valley. Second, as discussed before the active C atom #1 is the terminal atom of a flexible chain. In this respect it has to be kept in mind that the surface shown in Fig. 5 is only the static surface of the PES analysis prior to CH_3 bombardment while the CH_3 locations are those at the end of the dynamic simulations.

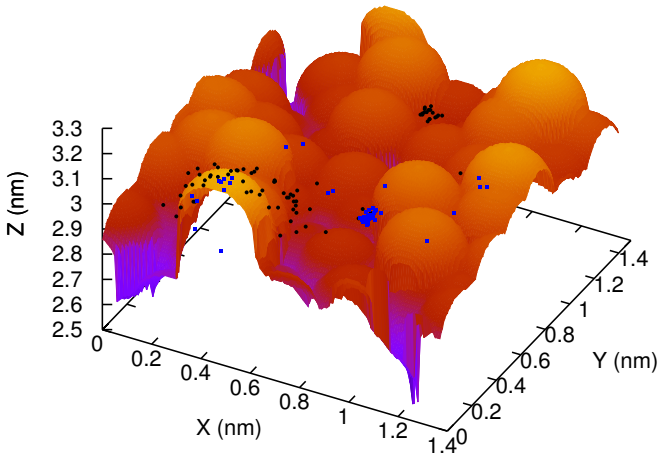

FIG. 5. Static surface of the virgin sample prior to CH_3 bombardment and the CH_3 locations at the end of the simulations. Solid circles: CH_3 locations above the initial surface, solid squares: CH_3 locations below the initial surface. The distributed sticking on the left front side (x∼0.4, y∼0.1) belongs to active carbon atom #1. The cluster of CH_3 sites in the center is carbon atom #2 (middle, x∼0.8, y∼0.6) and the cluster in the upper right part to #3 (upper right, x∼0.8, y∼1.2).

The reactivity of individual C atoms can be expressed as the ratio of CH_3 sticking events on individual active carbon atoms to the total number of sticking events on the surface. We call this 'fractional sticking'. The fractional sticking for each active C atom is plotted in Fig. 6. The higher the fractional sticking the higher is the reactivity of the atom (see Section V C for the discussion on reactivity). The shortest distance and the vertical distance of each of the active carbon atoms from the local surface are also shown in Fig. 6. For rough surfaces, the vertical distance can be significantly larger than the shortest distance. This is

here the case for atoms #6 to #11. For all atoms where a sticking event has happened, the shortest distance is approximately 0.18 nm from the local surface. This indicates that sticking happened on the top layer of active carbon atoms that are located at 0.18 nm below the surface (the potential cut-off for C-H interactions is 0.18 nm, recall Sect. IV B for the definition of surface). Slightly higher shortest distances of the active carbon atoms to the surface where sticking can occur are due to either the finite grid size or the thermal motion of the atoms.

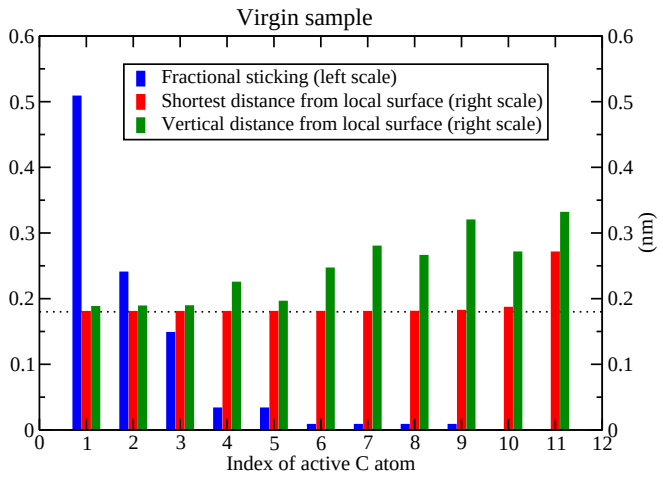

FIG. 6. Number of CH_3 sticking events for every individual active C atom normalized to the total number of sticking events (fractional sticking), shortest distance of the binding sites from the local surface, and vertical distance of the active C atoms from the local surface for the virgin sample.

B. Other Samples

The application of the algorithm to the H-exposed sample yielded 12 active carbon atoms. Nine of them were common to both the virgin and H-exposed samples. The active carbon atoms #1 and #2 of the virgin surface have disappeared on the H-exposed sample. A closer look at the sample showed that they became completely saturated due to hydrogenation and recombination. Sticking happened on all the nine active carbon atoms that are located ~ 0.18 nm below the local surface. No sticking was observed on the remaining three atoms that are within a distance of 0.4 nm from the surface. We have also observed three sticking events on carbon atoms in the thermostated region. Since there was no bombardment in this area, the active atoms in the thermostated region and the associated sticking events are not counted in any calculations.

For the H-saturated surface, the algorithm has identified 4 active carbon atoms. All the sticking happened on the three active carbon atoms that belong to the top layer. The fourth active carbon atom was located at 0.3 nm below the closest local surface. All these active carbon atoms were also identified in both the virgin and the H-exposed samples.

For the Ar-bombarded surface, the algorithm has identified 14 active carbon atoms within the sample (see Fig. 7). Among the identified ones, it has three in common with the virgin sample (#2, #5, #6 of the virgin sample corresponding to #5, #7 and #6 of the Ar-bombarded sample). The rest is created due to the argon bombardment events. This also means that 8 active carbon atoms of the virgin sample have disappeared.

Nearly 91% (474) of the sticking happened on ten active carbon atoms that have a shortest distance of ~ 0.18 nm from the local surface. Almost 7% (40) of the sticking happened on the active carbon atoms that are lying just outside the bombardment area (inside the thermostat). Similar to the H-exposed sample, here also we have not used these carbon atoms and the associated sticking events for any further calculations. The remaining 2% (11) were weak sticking events that we could not associate with any of the active carbon atoms. One sticking event was observed on the active carbon atom #11 which has a shortest distance of 0.21 nm from the local surface (Fig. 7). With a 0.01 nm grid this deviation is too large for a finite grid size effect and hence can only be attributed to the dynamic evolution of the surface. From the figure we also see that the shortest distance to the surface provides a good criterion to decide whether an active carbon atom may contribute to sticking. However, no such correlation can be derived for the vertical distance of active carbon atoms from the local surface. We conclude that the vertical distance is not the correct measure for estimating whether an active carbon atom contributes to sticking or not.

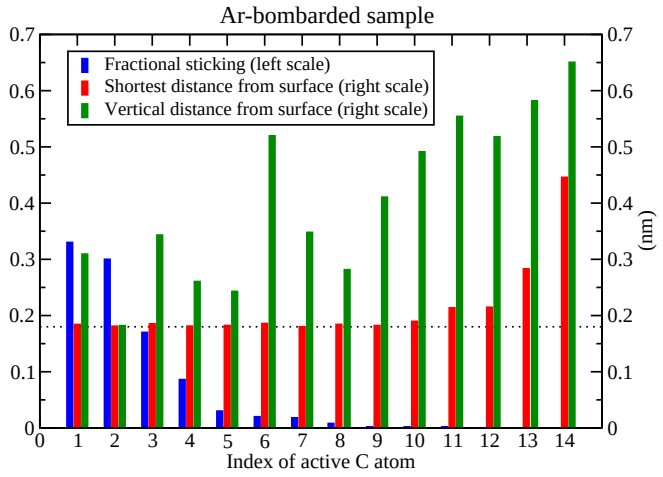

FIG. 7. Number of CH_3 sticking events for every individual active C atom normalized to the total number of sticking events (fractional sticking), shortest distance and vertical distance of the active C atoms from the local surface for the Ar-bombarded sample.

From the analysis of all the four samples we conclude that the shortest distance from the local surface seems to be a good estimate to decide whether an active carbon atom may contribute to sticking or not. Sticking happens on all the active carbon atoms that are on the top layer of the sample. From the analysis of the virgin sample we have also seen that the sticking is more localized at the valleys of the surface and the active atoms belonging to flexible hydrocarbon chains form a local hill where the

sticking is much more scattered.

C. Reactivity of Active Carbon Atoms

Although the sticking happens on all the active carbon atoms of the top layer for all the four samples, the number of radicals stuck on each C atom varied between 1 and 156 (out of 10000 bombardment events). This shows that the individual reactivity of the atoms changes considerably. In an attempt to understand what determines the reactivity of individual active C atoms, we take into account their type that we have already introduced in section IV C. The type and the number of active carbon atoms where a sticking event has happened are given in Tab. III. The number of sticking events associated with each of the active carbon atoms is given in parentheses.

As a reminder, our notation $i\mathrm{C}j\mathrm{H}^{(*)}$ means the respective carbon atom has bonds to $i \in \{1,\ldots,3\}$ carbon and $j \in \{0,\ldots,3-i\}$ hydrogen atoms. The asterisk, if present, indicates that one of the neighboring carbon atoms was also identified as active. If adjacent carbon atoms are active (2 or more) then the reactivity of the topmost one increases significantly and this is what we see in the cases of $2\mathrm{C}1\mathrm{H}^*$ and $3\mathrm{C}^*$: for example in the case of the virgin sample, the active C atoms #2 and #5 are bonded to each other and the atom #2, which is slightly above the atom #5, has 29 sticking compared to 4 sticking on atom #5. A similar observation can be made for atoms #3 and #10 of virgin sample, #1 and #9 of H-exposed sample and #5 and #11 of the Ar-bombarded sample. Hence only the one which is closest to the surface is counted in either of the $*$ types.

All the active carbon atoms listed in Tab. III are in the top layer. In addition to the requirement that an active carbon must be a surface atom to make sticking possible, we conclude from Tab. III that its type plays an important role in determining the reactivity. We see that if the active carbon atom is a terminal one (1C1H and 1C2H) such that it can readjust in the local neighborhood or of 2C type then it has a higher reactivity. If the active carbon atom belongs to any of two the $*$ types then it also has a higher reactivity. We call these five types collectively 'highly reactive' carbon atoms. They are denoted as 'H' in Tab. III. The other active types (2C1H and 3C) show very low reactivity and are indicated by 'L'. In the case of the virgin sample, 90% of the sticking events (109 out of 121) are on the highly active carbon atoms #1, #2 and #3. On the H-exposed sample nearly 80% (65 out of 81 accounted sticking events) of the sticking happened on the highly reactive atoms #1 to #4.

As expected the total number of sticking events on the H-exposed sample (84) was lower than that on the virgin sample (122). However, contrary to our expectation, this is not due to the reduction in the number of highly reactive carbon atoms: the total number of active carbon atoms where a sticking event has happened stayed constant and one of the low reactive ones even was converted to a highly reactive type. On the H-saturated sample indeed the number of active carbon atoms was reduced and all are of low reactive types, i.e., 2C1H and 3C types. The total number of sticking events in this case is also very low (13 out of

TABLE III. The type and index of active carbon atoms for all the four samples. The number of sticking events associated with each carbon atom is given in parentheses. The asterisk indicates that one of the neighboring carbon atoms are also active. The reactivity of the type is indicated by R. The highly reactive carbon atoms are indicated by H and the low reactive ones are by L. The last line shows the total number of active C atoms of all the types and the sum of all the sticking events associated with them.

Type	Index and (number of sticking events)				R
	Virgin	H-exposed	H-saturated	Ar-bombarded	
1C1H	1 (62)	4 (6)	-	7 (10)	H
1C2H	-	-	-	1 (156), 4 (41)	H
2C	-	-	-	2 (142), 3 (81)	H
2C1H	5 (4), 6, 7, 8, 9 (1 each)	6 (4), 7 (2)	1 (9)	8 (9), 11 (1)	L
2C1H*	2 (29)	2 (16), 3 (15)	-	5 (15)	H
3C	4 (4)	5 (6), 8 (2), 9 (2)	2 (2), 3 (2)	9 (4), 10 (1)	L
3C*	3 (18)	1 (28)	-	6 (14)	H
Total	9 (121)	9 (81)	3 (13)	11 (474)	

10,000 bombardment events).

For the Ar-bombarded sample, 94% of the sticking (459 out of 474 accounted sticking events) was on the highly reactive carbon atoms #1 to #7. We have already seen that the surface hydrogen content reduces due to argon bombardment (cf. Fig 3). Along with that, not only the number of active C atoms increases but also their type changes. The highly reactive types 1C2H and 2C are observed only in the case of the Ar-bombarded sample. In fact, the active carbon atoms #1, #2 and #3 show the highest individual sticking among all the investigated carbon atoms. This means that Ar-bombardment not only increases the number of active carbon atoms, from 11 on the virgin sample to 14, but also results in active carbon atoms with a much higher individual reactivity. This enhances the total sticking coefficient of the surface.

Altogether in all the four samples a majority (18 out of 30) of the active atoms are 2C1H and 3C types but their contribution to the total sticking is rather low (56 out of 689 events altogether). If there are no highly reactive C atoms on the surface, for example in the case of the H-saturated sample, then the total reactivity of the surface reduces drastically. In the other three cases more than 80% of the sticking happened on the highly reactive carbon atoms (1C1H, 1C2H, 2C, 2C1H* and 3C*). From Tab. III we also see that for the same type of carbon atom different surfaces shows different number of sticking events. The 1C1H type on the virgin sample has 62 sticking events, whereas only 6 events were seen on the H-exposed sample. We speculate that the difference in sticking is due to the fact that on the virgin sample the 1C1H type (active carbon atom #1) is the termination of a

highly flexible 6 carbon chain. On the other two surfaces this was just a terminal carbon atom.

The 1C2H and 2C types are only observed (2 each) in the case of Ar-bombarded sample. However, the sticking on each of them varied significantly (41 and 156 on two 1C2H type and 81 and 142 on two 2C type). Although 2C1H* and 3C* show similar sticking on all the three surfaces, the variation among them is more than what we would expect from statistical uncertainty. In other words the cross-section of individual active carbon atoms depends not only on their type but also on other local surface properties. Important factors could be their local hydrogen environment that leads to steric hindrance and the flexibility of the local carbon environment. Such an analysis would require an even larger number of surfaces with a sufficient number of reactive types and different local environments.

In principle, the potential energy analysis presented in this paper is a general technique that is applicable to the analysis of energy landscapes regardless of their origin, be it ab inito methods, DFT or MD and the generic approach and the involved speed-up is independent of the potential details. However, the selection rules for the algorithm such as the potential cut-off and the required grid size depend on the specifics of the potential. The Brenner potential used in the present article is not suitable for simulating aromatic rings. It is well known that the sp^2 phase in amorphous (hydro) carbon films forms clusters of aromatic rings [2, 53]. The present algorithm does not distinguish between a C=C–C pattern in an aromatic ring and a linear C–C–C structure as the central carbon atom in both cases would be classified as a 2C site. Hence one has to be cautious in applying to sp^2 rich carbon films. The present form of the algorithm is limited to systems that contain only carbon and hydrogen. Although the algorithm is capable of finding the dangling bonds in all covalent systems, it is currently not capable of identifying the binding partner of CH_3 in presence of other elements. For example if nitrogen or oxygen is present in the vicinity of an identified dangling bond, the present algorithm cannot find out whether it belongs to carbon, nitrogen or oxygen. Apart from that, in such cases polarity of such bonds will have to be taken into account by using appropriate simulation tools. It will be interesting to extend the present study to other hydrocarbon radicals to explore the differences in the selection criteria and the reactivity of the binding sites.

VI. CONCLUSIONS

We have investigated the nature of sticking locations for CH_3 radicals on realistic a-C:H film surfaces using molecular dynamics simulations. A combined molecular dynamics and potential energy analysis study reveals that of all the dangling bonds present in the film, only a few qualify as a binding site for a CH_3 radical. The factors that decide whether a dangling bond is a binding site or not are: (a) the type of the carbon atom that posses the binding site, which is decided by their bonding partner, (b) the distance from the local surface and (c) the local environment.

The binding sites are identified by successive elimination of the attractive sites obtained from the potential energy analysis of a-C:H films using a hydrogen atom as a test particle. In the first stage, the depth of the attractive potential well is used to discriminate physisorption sites and dangling bonds. Rather weak physisorption sites (PE ≥ -0.6 eV) did not contribute to any of the sticking events. Whether a dangling bond (PE ≤ -0.9 eV) contributes to sticking and hence becomes a binding site or not is decided by the *type* of the carbon atom it belongs to. The type *i*C*j*H is defined by the number i of C atoms and j of H atoms it has bonds with.

Only if the carbon atom associated with a dangling bond fulfills one of the following three conditions is it considered as a binding site: (i) the carbon atom is of 1C1H, 1C2H or 2C type, (ii) at least one of its adjacent carbon atoms also possesses a dangling bond, denoted by an asterisk, (applies to 2C1H* and 3C*), or (iii) the carbon atom is a part of a flexible hydrocarbon chain (applies to 2C1H and 3C types). A carbon atom with a binding site is called an *active carbon atom*. Only on active carbon atoms that are in the top layer of the film (~ 0.18 nm from the local surface) does sticking occur.

The active carbon atoms fulfilling conditions (i) or (ii) are highly reactive and are responsible for more than 80% of the sticking on the virgin, the H-exposed and the Ar-bombarded surfaces. The sticking probabilities on the corresponding surfaces are 1.2×10^{-2}, 8.4×10^{-3} and 5.3×10^{-2} respectively. The active carbon atoms that fulfill condition (iii), i.e., 2C1H or 3C types that are part of a hydrocarbon chain are of low reactive type. The H-saturated surface has only such low reactive types and the corresponding sticking probability was the lowest (1.3×10^{-3}) among all the four investigated samples.

An additional insight gained from the investigation is that for the same type of highly reactive carbon atom, the presence of a very flexible environment, such as long hydrocarbon chains, can strongly increase the sticking probability on it. This is assumed to be the reason for the dramatically different number of sticking events on the active carbon atoms of 1C1H type on the virgin surface (62 events) and the H-exposed surface (6 events).

The study also revealed that, contrary to the expectation, the reduction in the sticking coefficient is not always a direct consequence of the reduction in the number of active carbon atoms. Even if the number of active carbon atoms increases like in the case of the H-exposed sample, the local neighborhood can prevent radical incorporation and consequently reduces the sticking coefficient. The hydrogen depletion and subsequent local rearrangement due to energetic argon bombardment, not only increased the number of active carbon atoms but also created more highly reactive types. This resulted in the high sticking coefficient of the Ar-bombarded sample. This could be the atomistic explanation for the experimentally observed high reactivity of the ion-bombarded surfaces [8, 18, 54].

ACKNOWLEDGMENT

P.N. Maya thanks Dr. S.P. Deshpande, Dr. M. Warrier and Dr. C. Hopf for useful discussions.

REFERENCES

[1] J. C. Angus, P. Koidl, and S. Domitz. Plasma deposited thin films. page 89. CRC Press, 1986.

[2] J. Robertson. Diamond-like amorphous carbon. *Mat. Sci. Eng. Reports*, 37:129–281, 2002.

[3] A. Grill. Diamond-like carbon: State of the art. *Diamond Relat. Mater.*, 8:428, 1999.

[4] J. Robertson. Ultrathin carbon coatings for magnetic storage technology. *Thin Solid Films*, 383:81, 2001.

[5] R. Hauert. An overview on the tribological behavior of diamond-like carbon in technical and medical applications. *Tribology International*, 37:991–1003, 2004.

[6] A. H. Lettington. Applications of diamond-like carbon thin films. *Carbon*, 36:555, 1998.

[7] V.-M. Tiainen. Amorphous carbon as a bio-mechanical coating mechanical properties and biological applications. *Diamond Relat. Mater.*, 10:153–160, 2001.

[8] W. Jacob. Surface reactions during growth and erosion of hydrocarbon films. *Thin Solid Films*, 326:1–42, 1998.

[9] T. Schwarz-Selinger, A. von Keudell, and W. Jacob. Plasma chemical vapor deposition of hydrocarbon films: The influence of hydrocarbon source gas on the film properties. *J. Appl. Phys.*, 86:3988, 1999.

[10] W. Jacob, C. Hopf, M. Meier, and T. Schwarz-Selinger. *Nuclear Fusion Research – Understanding Plasma–Surface Interaction*, chapter 11. Interaction of low-energy ions and hydrocarbon radicals with carbon surfaces, pages 249–285. Springer Series in Chemical Physics. Springer Verlag, Berlin, 2005.

[11] J. Roth, E. Tsitrone, A. Loarte, Th. Loarer, G. Counsell, R. Neu, V. Philipps, S. Brezinsek, M. Lehnen, P. Coad, Ch. Grisolia, K. Schmid, K. Krieger, A. Kallenbach, B. Lipschultz, R. Doerner, R. Causey, V. Alimov, W. Shu, O. Ogorodnikova, A. Kirschner, G. Federici, A. Kukushkin, EFDA PWI Task Force, ITER PWI Team, Fusion for Energy, and ITPA SOL/DIV. Recent analysis of key plasma wall interactions issues for ITER. *J. Nucl. Mater.*, 390–391:1–9, 2009.

[12] A. von Keudell, T. Schwarz-Selinger, and W. Jacob. Simultaneous interaction of methyl radicals and atomic hydrogen with amorphous hydrogenated carbon films. *J. Appl. Phys.*, 89:2979, 2001.

[13] C. Hopf, A. von Keudell, and W. Jacob. Direct verification of the ion-neutral synergism during hydrocarbon film growth. *J. Appl. Phys.*, 93:3352–3358, 2003.

[14] A. von Keudell, T. Schwarz-Selinger, M. Meier, and W. Jacob. Direct identification of the synergism between methyl radicals and atomic hydrogen during growth of amorphous hydrogenated carbon films. *Appl. Phys. Lett.*, 76:676, 2000.

[15] A. von Keudell. Formation of polymer-like hydrocarbon films from beams of methyl radicals and atomic hydrogen. *Thin Solid Films*, 402:1–37, 2002.

[16] M. Meier, R. Preuss, and V. Dose. Interaction of CH_3 and H with amorphous hydrocarbon surfaces: Estimation of reaction cross sections using bayesian probability theory. *New J. Phys.*, 5:133.1, 2003.

[17] A. von Keudell, M. Meier, and C. Hopf. Growth mechanisms of a–C:H films. *Diamond Relat. Mater.*, 11:969, 2002.

[18] C. Hopf, W. Jacob, and A. von Keudell. Ion-induced surface activation, chemical sputtering, and hydrogen release during plasma-assisted hydrocarbon film growth. *J. Appl. Phys.*, 97:094904 (6pp), 2005.

[19] Yoshiko Miyagawa, Hiroshi Nakadate, Masaaki Tanaka, and Soji Miyagawa. Dynamic MC simulation of DLC films synthesis by PBII. *Surf. Coat. Technol.*, 156:87–91, 2002.

[20] Y. Miyagawa, H. Nakadate, M. Ikeyama, S. Nakao, and S. Miyagawa. Dynamic MC simulation for a-C:H deposition in methane plasma based on subplantation model. *Diamond Relat. Mater.*, 12:927–930, 2003.

[21] C.C. Battaile, D.J. Srolovitz, and J.E. Butler. Morphologies of diamond films from atomic-scale simulations of chemical vapor deposition. *Diamond Relat. Mater.*, 6:1198–1206, 1997.

[22] P. N. Maya, S. P. Deshpande, and M. Warrier. Monte carlo modeling of structure and porosity of codeposited layers. *Contrib. Plasma Phys.*, 46(5-7):757–762, 2006.

[23] G. Zilibotti, S. Corni, and M. C. Righi. Formation energy of dangling bonds on hydrogenated diamond surfaces: A first-principles study. *Phys.Rev.B*, 85:033406, 2012.

[24] Ying Dai, Baibiao Huang, and Dadi Dai. The role of dangling-bond, hydrogen and adsorbate in diamond surface conduction. *Diamond Relat. Mater.*, 12:15–19, 2003.

[25] D.A. Alman and D.N. Ruzic. Molecular dynamics calculation of carbon/hydrocarbon reflection coefficients on a hydrogenated graphite surface. *J. Nucl. Mater.*, 313–316:182–186, 2003.

[26] D. A. Alman and D. N. Ruzic. Molecular dynamics simulation of hydrocarbon reflection and dissociation coefficients from fusion-relevant carbon surfaces. *Phys. Scripta*, T111:145–151, 2004.

[27] K. Tichmann, U. von Toussaint, T. Schwarz-Selinger, and W. Jacob. Determination of the sticking probability of hydrocarbons on an amorphous hydrocarbon surface. *Phys. Scripta*, T138:014015 (4pp), 2009.

[28] K. Tichmann, U. von Toussaint, and W. Jacob. Determination of the sticking coefficient of energetic hydrocarbon molecules by molecular dynamics. *J. Nucl. Mater.*, 420:291–296, 2012.

[29] E.D. de Rooij, A.W. Kleyn, and W.J. Goedheer. Sticking of hydrocarbon radicals on different amorphous hydrogenated carbon surfaces: a molecular dynamics study. *Phys. Chem. Chem. Phys.*, 12:14067–14075, 2010.

[30] Erik Neyts, A. Bogaerts, R. Gijbels, J. Benedikt, and M.C.M. van de Sanden. Molecular dynamics simulations for the growth of diamond-like carbon films from low kinetic energy species. *Diamond Relat. Mater.*, 13:1873–1881, 2004.

[31] E. Neyts, A. Bogaerts, and M.C.M. van de Sanden. Unraveling the deposition mechanism in a-C:H thin-film growth: A molecular-dynamics study for the reaction behavior of c_3 and c_3h radicals with a-C:H surfaces. *J. App. Phys.*, 99(014902):1–8, 2006.

[32] E. Neyts, A. Bogaerts, and M.C.M. van de Sanden. Reaction mechanisms and thin a-C:H film growth from low energy hydrocarbon radicals. *J. Phys. Conf. Series*, 86(012020):1–15, 2007.

[33] H. U. Jäger and K. Albe. Molecular-dynamics simulations of steady-state growth of ion-deposited tetrahedral amorphous carbon films. *J. Appl. Phys.*, 88:1129, 2000.

[34] A.Yu. Belov and H. U. Jäger. Simulation of the non-equilibrium processes for tetrahedral amorphous carbon: Deposition and structural relaxation. *Nucl. Instr. and Meth.in Phys. Res. B*, 202:242–248, 2003.

[35] H. U. Jäger and M. Weiler. Molecular dynamics studies of a-c:h film growth by energetic hydrocarbon molecule impact. *Diamond Relat. Mater.*, 7:858–863, 1998.

[36] A. Sharma, R. Schneider, U. von Toussaint, and K. Nordlund. Hydrocarbon radicals interaction with amorphous carbon surfaces. *J. Nucl. Mater.*, 363–365:1283–1288, 2007.

[37] P. Träskelin, E. Salonen, K. Nordlund, A.V. Krasheninnikov, J. Keinonen, and C.H. Wu. Molecular dynamics simulation of CH_3 sticking on carbon surfaces. *J. Appl. Phys.*, 93:1826–1831, 2003.

[38] P. Träskelin, E. Salonen, K. Nordlund, A.V. Krasheninnikov, J. Keinonen, and C.H. Wu. Molecular dynamics simulations of CH_3 sticking on carbon first wall structures. *J. Nucl. Mater.*, 313–316:52–55, 2003.

[39] P. Träskelin, E. Salonen, K. Nordlund, J. Keinonen, and C.H. Wu. Molecular dynamics simulation of CH_3 sticking on carbon surfaces, angular and energy dependence. *J. Nucl. Mater.*, 334:65–70, 2004.

[40] D. R. Alfonso and S. E. Ulloa. Molecular-dynamics simulations of methyl-radical deposition on diamond (100) surfaces. *Phys. Rev. B*, 48:12235–12239, 1993.

[41] D.R. Alfonso, S.E. Ulloa, and D.W. Brenner. Hydrocarbon adsorption on a diamond (100) stepped surface. *Phys. Rev. B*, 49:4948, 1994.

[42] K. Nordlund and J. Keinionen. Formation of ion irradiation induced small-scale defects on graphite surfaces. *Phys. Rev. Lett.*, 77:699, 1996.

[43] D. W. Brenner. Empirical potential for hydrocarbons for use in simulating the chemical vapor deposition of diamond films. *Phys. Rev. B*, 42:9458–9471, 1990.

[44] D. W. Brenner. Erratum:empirical potential for hydrocarbons for use in simulating the chemical vapor deposition of diamond films. *Phys. Rev. B*, 46:1948–1948, 1992.

[45] D. W. Brenner, Olga A Shenderova, Judith A Harrison, Steven J Stuart, Boris Ni, and Susan B Sinnott. A second-generation reactive empirical bond order (rebo) potential energy expression for hydrocarbons. . *Phys.: Condens. Matter*, 14:783–802, 2002.

[46] P de Sainte Claire, K. Song, W. L. Hase, and D. W. Brenner. Comparison of ab initio and empirical potentials for h-atom association with diamond surfaces. *J. Phys. Chem.*, 100:1761–1766, 1996.

[47] G Lucas, M Bertolus, and L Pizzagalli. An environment-dependent interatomic potential for silicon carbide: calculation of bulk properties, high-pressure phases, point and extended defects, and amorphous structures. *J. Phys.: Condens. Matter*, 100:035802–1–15, 2010.

[48] T. Kumagai, S. Hara, J. Choi, S. Izumi, and T. Kato. Development of empirical bond-order-type interatomic potentialfor amorphous carbon structures. *J. Appl. Phys.*, 105:064310–1–10, 2009.

[49] P. N. Maya, U. von Toussaint, and C. Hopf. Synergistic erosion process of hydrocarbon films: A molecular dynamics study. *New J. Phys.*, 10:023002 (15pp), 2008.

[50] J.K. Walters and R.J. Newport. The atomic scale structure of amorphous hydrogenated carbon. *J. Phys.: Condens. Matter*, 7:1755–1769, 1995.

[51] H. J. C. Berendsen, J. P. M. Postma, W. F. Van Gunsteren, A. DiNola, and J. R. Haak. Molecular dynamics with coupling to an external bath. *J. Chem. Phys.*, 81(8):3684–3690, 1984.

[52] C. Hopf, A. von Keudell, and W. Jacob. The influence of hydrogen ion bombardment on plasma-assisted hydrocarbon film growth. *Diamond Relat. Mater.*, 12:85–89, 2003.

[53] J. Robertson. Structural models for a–C and a–C:H. *Diamond Relat. Mater.*, 4:297, 1995.

[54] A. von Keudell and W. Jacob. Elementary processes in plasma surface interaction: H-atom and ion-induced chemisorption of methyl on hydrocarbon film surfaces. *Prog. Surf. Sci.*, 76:21, 2004.